PNAS
www.pnas.org

Supplementary Information for

Dendritic computations captured by an effective point neuron model

Songting Li, Nan Liu, Xiaohui Zhang, David McLaughlin, Douglas Zhou, and David Cai

X. Z. xhzhang@bnu.edu.cn
D.M. david.mclaughlin@nyu.edu
D.Z. zdz@sjtu.edu.cn

This PDF file includes:

Supporting Information Text

Derivation of the synaptic integration current. In the main text, we have demonstrated that the point neuron model without the synaptic integration current (Eqs. 1 and 2 in the main text) does not suffice to characterize the somatic voltage dynamics of a spatial neuron with dendrites. In addition, using both electrophysiological experiments and realistic neuron simulations, we have obtained a novel synaptic integration current form being capable of characterizing the synaptic current arriving at the soma when the spatial neuron receives synaptic inputs on its dendrites. A bilinear conductance relation is further obtained in experiments and realistic neuron simulations. Here we theoretically explain the origin of the synaptic integration current by performing the static two-port analysis.[1,2,3] When a neuron receives static synaptic inputs, the electrical circuit representation of the neuron and the corresponding variables used in our analysis are shown in Fig. S0 below.

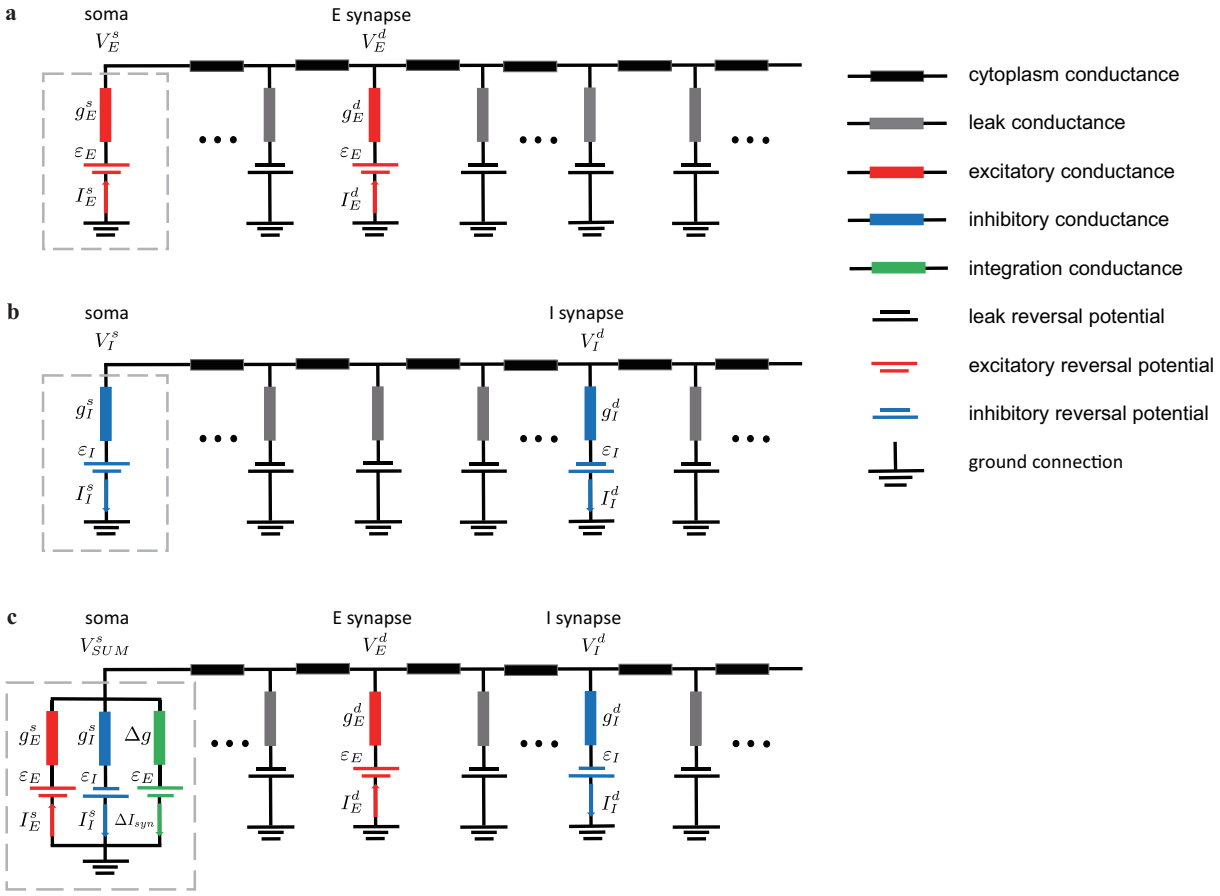

Fig. S0. Schematic diagram of the electrical circuit representation of a neuron when (**a**) an individual E input is received on the dendrite, (**b**) an individual I input is received on the dendrite, and (**c**) a pair of E and I inputs are received on the dendrite. The dashed grey boxes indicate the effective inputs received at the soma mapped from the local inputs on the dendrite (see text for details).

When a spatial neuron receives an excitatory (E) input on the dendrite, the local synaptic current on the dendrite I_E^d can be characterized by Ohm's law,

$$I_E^d = g_E^d(\varepsilon_E - V_E^d), \quad [1]$$

where g_E^d is the local E conductance on the dendrite, ε_E is the E reversal potential, and V_E^d is the local membrane potential on the dendrite. Here the superscript "d" emphasizes the quantities on the dendrite.

Based on Ohm's law, the local membrane potential V_E^d can be computed by

$$V_E^d = K_{EE} I_E^d, \quad [2]$$

where K_{EE} is the resistance at the E synapse. Therefore, combining Eqs. 1-2, the local membrane potential V_E^d is expressed as

$$V_E^d = \frac{g_E^d K_{EE} \varepsilon_E}{1 + g_E^d K_{EE}}. \quad [3]$$

Similarly, the excitatory postsynaptic potential (EPSP) V_E^s measured at the soma in response to the excitatory synaptic current I_E^d on the dendrite can be computed by

$$V_E^s = K_{ES} I_E^d, \tag{4}$$

where K_{ES} is the transfer resistance between the E synapse and the soma. The combination of Eqs. 1-4 yields the somatic membrane potential in response to the E input on the dendrite,

$$V_E^s = \frac{g_E^d K_{ES} \varepsilon_E}{1 + g_E^d K_{EE}}. \tag{5}$$

Now if we denote the synaptic current arriving at the soma as I_E^s that is induced by the synaptic current I_E^d (Eq. 1) from the dendrite, then based on Ohm's law, the synaptic current at the soma can be derived as

$$I_E^s = \frac{V_E^s}{K_{SS}}, \tag{6}$$

where K_{SS} is the resistance at the soma, the superscript "s" emphasizes the quantities at the soma.

If we further denote the E conductance measured at the soma as g_E^s, then g_E^s shall also obey Ohm's law

$$g_E^s = \frac{I_E^s}{\varepsilon_E - V_E^s}, \tag{7}$$

From Eqs. 5-7, we can obtain an expression for the E conductance g_E^s at the soma,

$$g_E^s = \frac{g_E^d K_{ES}}{K_{SS}\left[1 + g_E^d (K_{EE} - K_{ES})\right]} \tag{8}$$

Similarly, when a spatial neuron receives an inhibitory (I) input on its dendrites, the somatic membrane potential in response to the I input on the dendrite and the I conductance g_I^s measured at the soma can be derived as

$$V_I^s = \frac{g_I^d K_{IS} \varepsilon_I}{1 + g_I^d K_{II}}, \tag{9}$$

$$g_I^s = \frac{g_I^d K_{IS}}{K_{SS}\left[1 + g_I^d (K_{II} - K_{IS})\right]}, \tag{10}$$

where g_I^d is the local I conductance on the dendrite, K_{IS} is the transfer resistance between the I synaptic site and the soma, and K_{II} and K_{SS} are the resistances at the I synapse and the soma, respectively.

If we measure the E and I conductances g_E^s and g_I^s at the soma, from Eqs. 8 and 10, we are able to infer the local E and I conductances on the dendrite g_E^d and g_I^d as

$$g_E^d = \frac{g_E^s K_{SS}}{K_{ES} - g_E^s K_{SS}(K_{EE} - K_{ES})}, \tag{11}$$

$$g_I^d = \frac{g_I^s K_{SS}}{K_{IS} - g_I^s K_{SS}(K_{II} - K_{IS})}. \tag{12}$$

Now given a pair of E and I synaptic inputs on the dendrites of the spatial neuron with the same input locations and strengths as given separately, by Ohm's law, we have the local E and I synaptic currents on the dendrite

$$I_E^d = g_E^d(\varepsilon_E - V_E^d), \tag{13}$$

$$I_I^d = g_I^d(\varepsilon_I - V_I^d). \tag{14}$$

In Eqs. 13-14, the local membrane potentials measured at the E synapse V_E^d and at the I synapse V_I^d can be obtained as follows,

$$V_E^d = K_{EE} I_E^d + K_{IE} I_I^d, \tag{15}$$

$$V_I^d = K_{EI} I_E^d + K_{II} I_I^d. \tag{16}$$

By solving Eqs. 13-16, we can obtain the local synaptic currents on the dendrite as

$$I_E^d = \frac{g_E^d \varepsilon_E + g_E^d g_I^d (K_{II}\varepsilon_E - K_{EI}\varepsilon_I)}{1 + g_E^d K_{EE} + g_I^d K_{II} + g_E^d g_I^d (K_{EE}K_{II} - K_{EI}^2)}, \tag{17}$$

$$I_I^d = \frac{g_I^d \varepsilon_I + g_E^d g_I^d (K_{EE}\varepsilon_I - K_{EI}\varepsilon_E)}{1 + g_E^d K_{EE} + g_I^d K_{II} + g_E^d g_I^d (K_{EE}K_{II} - K_{EI}^2)}. \tag{18}$$

By Ohm's law together with the local synaptic current expressions (17-18), we can further solve the membrane potential at the soma as

$$\begin{aligned} V^s_{SUM} &= K_{ES} I^d_E + K_{IS} I^d_I \\ &= \frac{g^d_E K_{ES}\varepsilon_E + g^d_I K_{IS}\varepsilon_I + g^d_E g^d_I \left[\varepsilon_E (K_{II}K_{ES} - K_{IS}K_{EI}) + \varepsilon_I (K_{EE}K_{IS} - K_{ES}K_{EI})\right]}{1 + g^d_E K_{EE} + g^d_I K_{II} + g^d_E g^d_I (K_{EE}K_{II} - K^2_{EI})}, \end{aligned} \tag{19}$$

V^s_{SUM} has been referred to as the summed somatic potential (SSP) in the main text.

On the one hand, by using the SSP expression (19), we can obtain the summed somatic current (SSC) denoted as $I^s_{SUM} = V^s_{SUM}/K_{SS}$; on the other hand, by using Eqs. 8, 10 and 19, we can reconstruct the EPSC and IPSC at the soma as $I^s_E = g^s_E(\varepsilon_E - V^s_{SUM})$ and $I^s_I = g^s_I(\varepsilon_I - V^s_{SUM})$, respectively.

Through calculations, we can show that the SSC is not equal to the linear summation of the EPSC and the IPSC. The difference between them, i.e., the synaptic integration current, can be expressed as

$$\begin{aligned} \Delta I_{syn} &= I^s_{SUM} - I^s_E - I^s_I \\ &= \frac{g^d_E g^d_I (A + g^d_E B + g^d_I C + g^d_E g^d_I D)}{K_{SS}\left[1 + g^d_E (K_{EE} - K_{ES})\right]\left[1 + g^d_I (K_{II} - K_{IS})\right]\left[1 + g^d_E K_{EE} + g^d_I K_{II} + g^d_E g^d_I (K_{EE}K_{II} - K^2_{EI})\right]} \end{aligned}$$

where

$$\begin{aligned} A &= \varepsilon_E K_{IS}(K_{ES} - K_{EI}) + \varepsilon_I K_{ES}(K_{IS} - K_{EI}), \\ B &= \varepsilon_E \left[K_{ES}K_{IS}(K_{EE} - K_{ES}) + K_{EI}(K_{EI}K_{ES} - K_{EE}K_{IS})\right] + \varepsilon_I K_{EE}K_{ES}(K_{IS} - K_{EI}), \\ C &= \varepsilon_I \left[K_{ES}K_{IS}(K_{II} - K_{IS}) + K_{EI}(K_{EI}K_{IS} - K_{II}K_{ES})\right] + \varepsilon_E K_{II}K_{IS}(K_{ES} - K_{EI}), \\ D &= \varepsilon_E \left[K^2_{EI}K_{ES}(K_{II} - K_{IS}) + K_{EE}K_{II}K_{IS}(K_{ES} - K_{EI}) + K_{ES}K_{IS}(K_{EI}K_{IS} - K_{ES}K_{II})\right] \\ &+ \varepsilon_I \left[K^2_{EI}K_{IS}(K_{EE} - K_{ES}) + K_{EE}K_{II}K_{ES}(K_{IS} - K_{EI}) + K_{ES}K_{IS}(K_{EI}K_{ES} - K_{IS}K_{EE})\right]. \end{aligned}$$

We note that, the synaptic integration current ΔI_{syn} vanishes when the E and I inputs are given at the soma, where $A = B = C = D = 0$. To the leading order of the input conductances, the synaptic integration current ΔI_{syn} is proportional to the multiplication of the E and I conductances on the dendrite,

$$\Delta I_{syn} = \frac{A}{K_{SS}} g^d_E g^d_I + o(g^d_E g^d_I). \tag{20}$$

If we further cast the synaptic integration current ΔI_{syn} in the form of Ohm's law, i.e., $\Delta I_{syn} = \Delta g(\varepsilon_E - V^s_{SUM})$, then we have

$$\begin{aligned} \Delta g &= \frac{\Delta I_{syn}}{\varepsilon_E - V^s_{SUM}} \\ &= \frac{A}{\varepsilon_E K_{SS}} g^d_E g^d_I + o(g^d_E g^d_I) \\ &= \frac{A K_{SS}}{\varepsilon_E K_{ES} K_{IS}} g^s_E g^s_I + o(g^s_E g^s_I) \end{aligned} \tag{21}$$

The second equality in Eq. 21 holds by viewing the ratio V^s_{SUM}/ε_E as a small variable and performing Taylor expansion to the first order. the The last equality in Eq. 21 holds because of Eqs. 11-12. We thus have explained the bilinear conductance relation observed in both the electrophysiological experiments and the realistic neuron simulations, i.e.,

$$\Delta g = \alpha_{EI} g^s_E g^s_I, \tag{22}$$

where the integration coefficient α_{EI} can be explicitly expressed as

$$\alpha_{EI} \approx K_{SS}\left(1 - \frac{K_{EI}}{K_{ES}}\right) + K_{SS}\frac{\varepsilon_I}{\varepsilon_E}\left(1 - \frac{K_{EI}}{K_{IS}}\right). \tag{23}$$

From the above expression (23), the integration coefficient α_{EI} vanishes when the E and I inputs are given at the soma. On account of the fact that ε_E is almost one order of magnitude larger than ε_I, the expression for the coefficient could be further simplified as

$$\alpha_{EI} \approx K_{SS}\left(1 - \frac{K_{EI}}{K_{ES}}\right).$$

Note that when the synaptic integration current is cast in the form of Ohm's law, the reversal potential is set to be the excitatory reversal potential ε_E. In fact, there is a degree of freedom for choosing the value of the reversal potential ε within the regime in which the ratio V^s_{SUM}/ε is much smaller than unity in order to make the Taylor expansion in Eq. 21 accurate. Correspondingly, the value of the integration coefficient α_{EI} depends on the choice of the reversal potential. However, we stress that the bilinear relation of the conductances (22) remains valid when choosing a different reversal potential value.

Spatial dependence of the integration coefficients. Note that the transfer function K_{EI} decreases as the distance between the E and I input locations increases, and K_{ES} decreases as the distance between the E input location and the soma increases. Therefore, in general, α_{EI} is large negative for E and I inputs spatially close to each other at distal dendrite and it is less negative for E and I inputs spatially separated away from each other at proximal dendrite. In particular, when the I input location is fixed on the dendritic trunk and the E input location is between the soma and the I input location, as the distance between the E input location and the soma increases, K_{EI} in the numerator increases while K_{ES} in the denominator decreases, hence the decrease of α_{EI}; when the E input location is further away from the soma than the I input location, as the distance between the E input location and the soma increases, both K_{EI} in the numerator and K_{ES} in the denominator decreases, hence α_{EI} remains almost constant. This explains the spatially asymmetric dependence of α_{EI} as observed in the realistic neuron simulation in the main text. In addition, in general, a neuron receives E inputs at distal dendrites while receives I inputs at proximal dendrites. In such a case, $K_{EI} > K_{ES}$. Therefore, α_{EI} is mostly negative.

Similarly, for a pair of inputs of the same type, we can also derive the bilinear form of the integration conductance as

$$\Delta g = \alpha_{Q_1Q_2} g^s_{Q_1} g^s_{Q_2},$$

where $Q = E, I$ represents the input type, and the integration coefficient $\alpha_{Q_1Q_2}$ can be expressed as

$$\begin{aligned} \alpha_{Q_1Q_2} &\approx \frac{K_{SS}\left[K_{Q_2S}(K_{Q_1S}-K_{Q_1Q_2})+K_{Q_1S}(K_{Q_2S}-K_{Q_1Q_2})\right]}{K_{Q_1S}K_{Q_2S}} \\ &= K_{SS}\left(2-\frac{K_{Q_1Q_2}}{K_{Q_1S}}-\frac{K_{Q_1Q_2}}{K_{Q_2S}}\right), \end{aligned} \quad [24]$$

from which we can see that $\alpha_{Q_1Q_2}$ is smaller for both inputs spatially close to each other at distal dendrite than those spatially separated away from each other at proximal dendrite. In particular, when the input location of Q_1 is fixed at the dendritic trunk while the input location of Q_2 is between the soma and that of Q_1, as the distance between the location of Q_2 and the soma increases, $K_{Q_1Q_2}$ increases but K_{Q_2S} decreases, hence the decrease of $\alpha_{Q_1Q_2}$; when the input location of Q_2 is further away from the soma than that of Q_1, as the distance between the location of Q_2 and the soma increases, both $K_{Q_1Q_2}$ and K_{Q_2S} decreases, which results in the decrease of the term $\frac{K_{Q_1Q_2}}{K_{Q_1S}}$ and almost no change of the term $\frac{K_{Q_1Q_2}}{K_{Q_2S}}$, hence the increase of $\alpha_{Q_1Q_2}$. This explains the spatially symmetric dependence of α_{EE} and α_{II} as observed in the realistic neuron simulation in the main text.

Bilinear dendritic integration rule. Previous experiments[2,4] showed that when a neuron receives a pair of E and I inputs, the SSP denoted by V_S can be well characterized by the following bilinear integration rule,

$$V^s_{SUM} = V^s_E + V^s_I + k_{EI} V^s_E V^s_I$$

where V^s_E and V^s_I denote the somatic EPSP and IPSP induced by the E and I inputs given alone respectively, and k_{EI} is the shunting coefficient independent of input strengths but dependent of input time and locations.

The above rule can be captured in the point neuron model by incorporating the synaptic integration current, and there is a one-to-one mapping between the shunting coefficient and the integration coefficient that can be derived in the following. Using the approximations of EPSP, IPSP, and SSP (Eqs. 5, 9 and 19), we can obtain the expression of the shunting coefficient k_{EI}

$$k_{EI} = \frac{V^s_{SUM} - V^s_E - V^s_I}{V^s_E V^s_I} \approx -\frac{K_{IE}}{K_{IS}\varepsilon_E} - \frac{K_{EI}}{K_{ES}\varepsilon_I}. \quad [25]$$

This explains the experimental observation that the SSP follows a bilinear integration rule with the shunting coefficient being independent of synaptic input strengths but dependent of the synaptic input locations. From Eqs. 23 and 25, we can directly obtain the one-to-one linear mapping between the integration coefficient and the shunting coefficient,

$$\alpha_{EI} \approx K_{SS}\varepsilon_I\left(\frac{\varepsilon_E + \varepsilon_I}{\varepsilon_E\varepsilon_I} + k_{EI}\right)$$

Therefore, the shunting coefficient k_{EI} exhibits the same spatially asymmetric feature as the integration coefficient α_{EI} as explained from our two-port analysis in the above.

Direction selectivity. Here we illustrate the capability of direction selectivity[5,6] of our point neuron model as discussed in the main text. For the sake of illustration, we consider the idealized case that the decay time constant of the membrane potential is extremely fast. In this case, on the one hand, if multiple E synaptic inputs are received by the neuron at different times, the last pair of E inputs will dominantly contribute to the somatic membrane potential at the time right after the last E input is received, because the membrane potential change induced by all the previous inputs decays rapidly. On the other hand, as an E input moves away from the soma towards the distal dendrite, K_{ES} becomes smaller. According to Eq. 24, α_{EE} in the point neuron model is larger negative for a pair of E inputs located at distal dendrite than that at proximal dendrite. Therefore,

the sequential activation of synaptic inputs in the direction from distal to proximal dendrites (whose effect will be dominated by the last pair of inputs at proximal dendrite with a small negative coefficient) gives rise to larger somatic response than the sequential activation of synaptic inputs in the reversed direction (whose effect will be dominated by the last pair of inputs at distal dendrite with a large negative coefficient). This enables the point neuron to perform the computation of direction selectivity.

Coincidence detection. Here we illustrate the capability of coincidence detection[7] of our point neuron model as discussed in the main text. For the sake of illustration, we consider the idealized case that a spatial neuron has two identical dendritic branches connecting to its soma. On the one hand, we have $K_{E_1S} = K_{E_2S}$ and a large $K_{E_1E_2}$ when two E inputs are received at the same location on a branch; on the other hand, we have $K_{E_1S} = K_{E_2S}$ and a small $K_{E_1E_2}$ when two E inputs are received on two different branches with equal distance to the soma. Therefore, from Eq. 24, α_{EE} in our point neuron model is large negative for two E inputs received on the same branch from one ear and it is nearly positive for two E inputs received on two separate branches from both ears. Therefore, the neuron's membrane potential may stay below the firing threshold when receiving two E inputs on the same branch, while it may cross the firing threshold when receiving two E inputs on two separate branches. This enables the point neuron to perform coincidence detection of inputs from both ears.

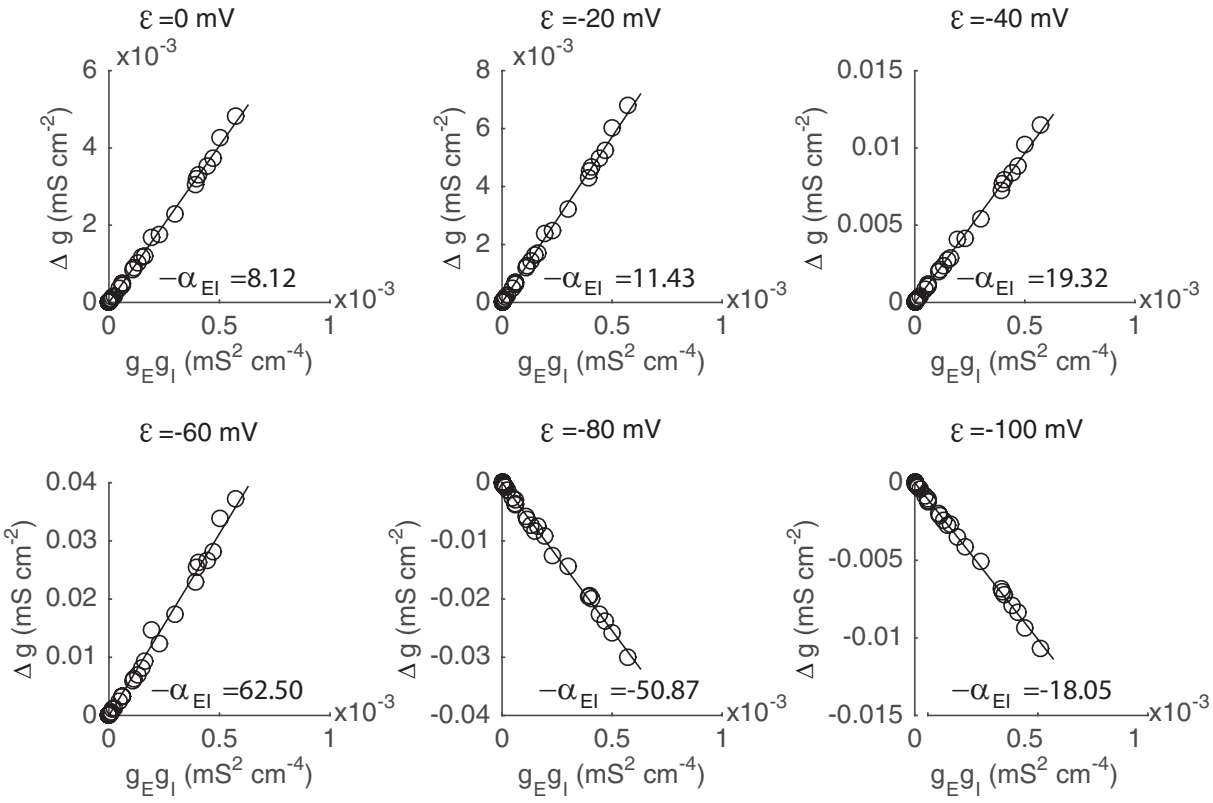

Fig. S1. The validity of the bilinear relation between Δg and the multiplication of g_E and g_I for different choice of reversal potential values ε in the synaptic integration current $\Delta I_{syn} = \Delta g(\varepsilon - V)$. The same data set is used here as that in Fig. 2c in the main text. The value of the reversal potential ranges from 0 mV to -100 mV. The corresponding integration coefficient value α_{EI} is specified within each figure panel with the unit of $\mathrm{k}\Omega \cdot \mathrm{cm}^2$.

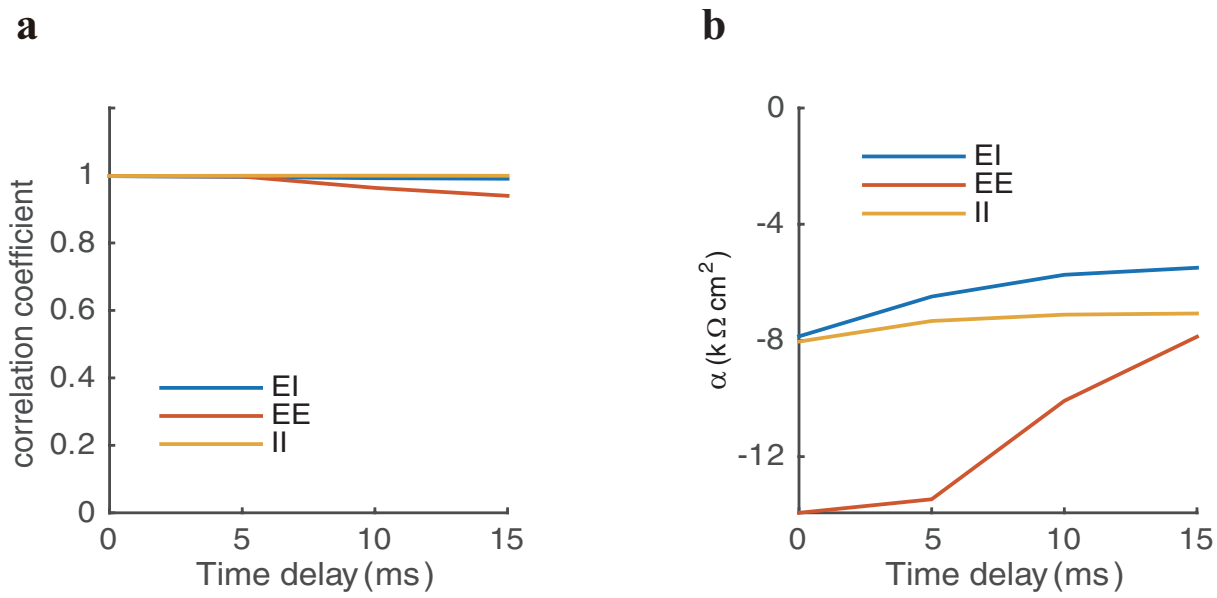

Fig. S2. The dependence of integration coefficients on the arrival time difference between a pair of E and I inputs, two E inputs, and two I inputs. **a**, the correlation coefficient between the integration conductance Δg and the product of the two individual conductances as a function of the time difference between the two inputs. **b**, the integration coefficient as a function of the time difference between the two inputs. All the data are measured at the peak time of an E conductance (for the EI and EE cases) or the peak time of an I conductance (for the II case).

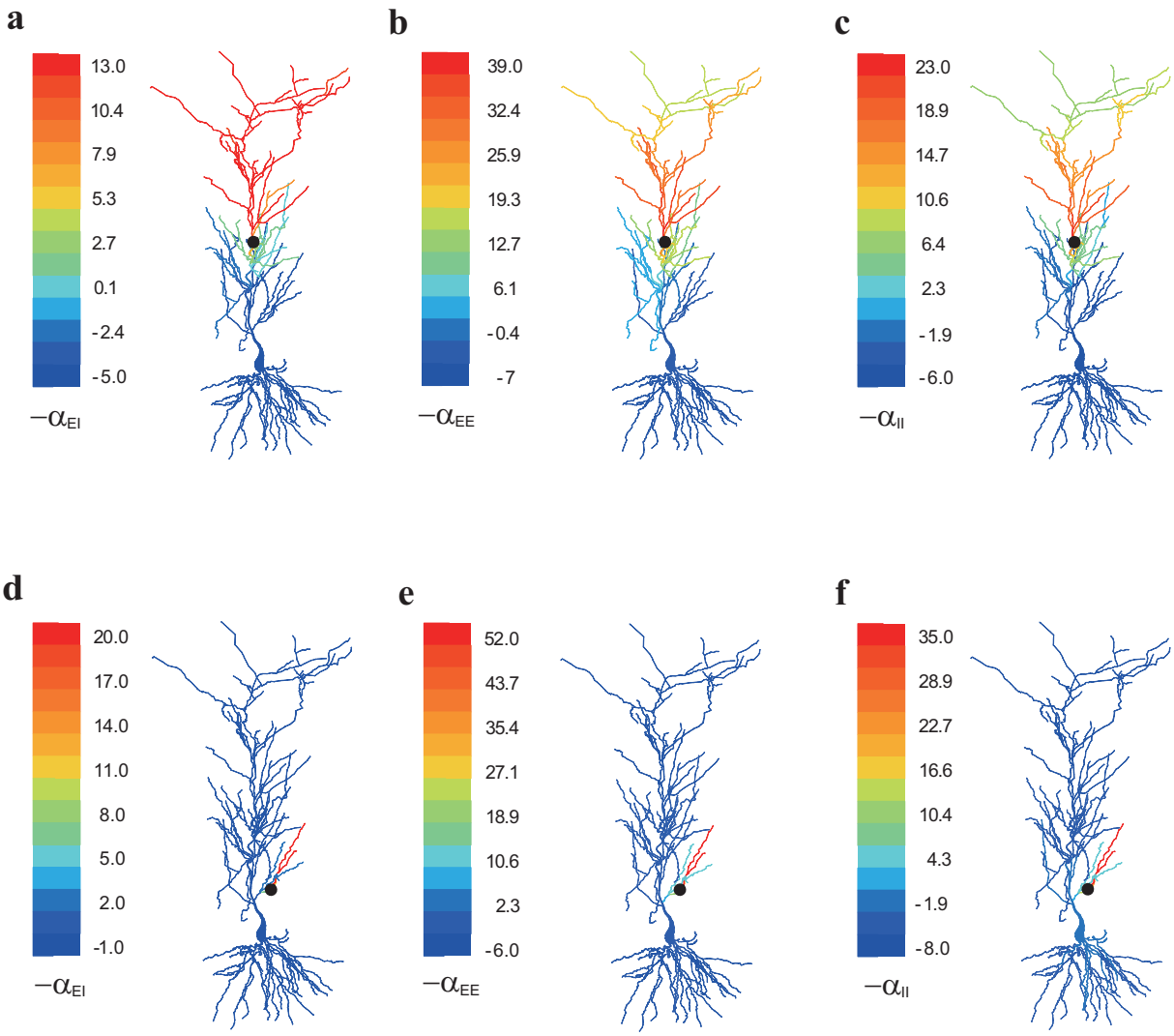

Fig. S3. The spatial profile of the integration coefficients in the whole dendrites. **a**, the spatial profile of $-\alpha_{EI}$ with the I input fixed at the dendritic trunk marked by the black dot and the E input scattered on the dendrites. **b-c**, the spatial profile of $-\alpha_{EE}$ and $-\alpha_{II}$ with one E (I) input fixed at the dendritic trunk marked by the black dot and the other E(I) input scattered on the dendrites. **d-f**, the same as **a-c** except that one input is fixed at a dendritic branch rather than at the dendritic trunk.

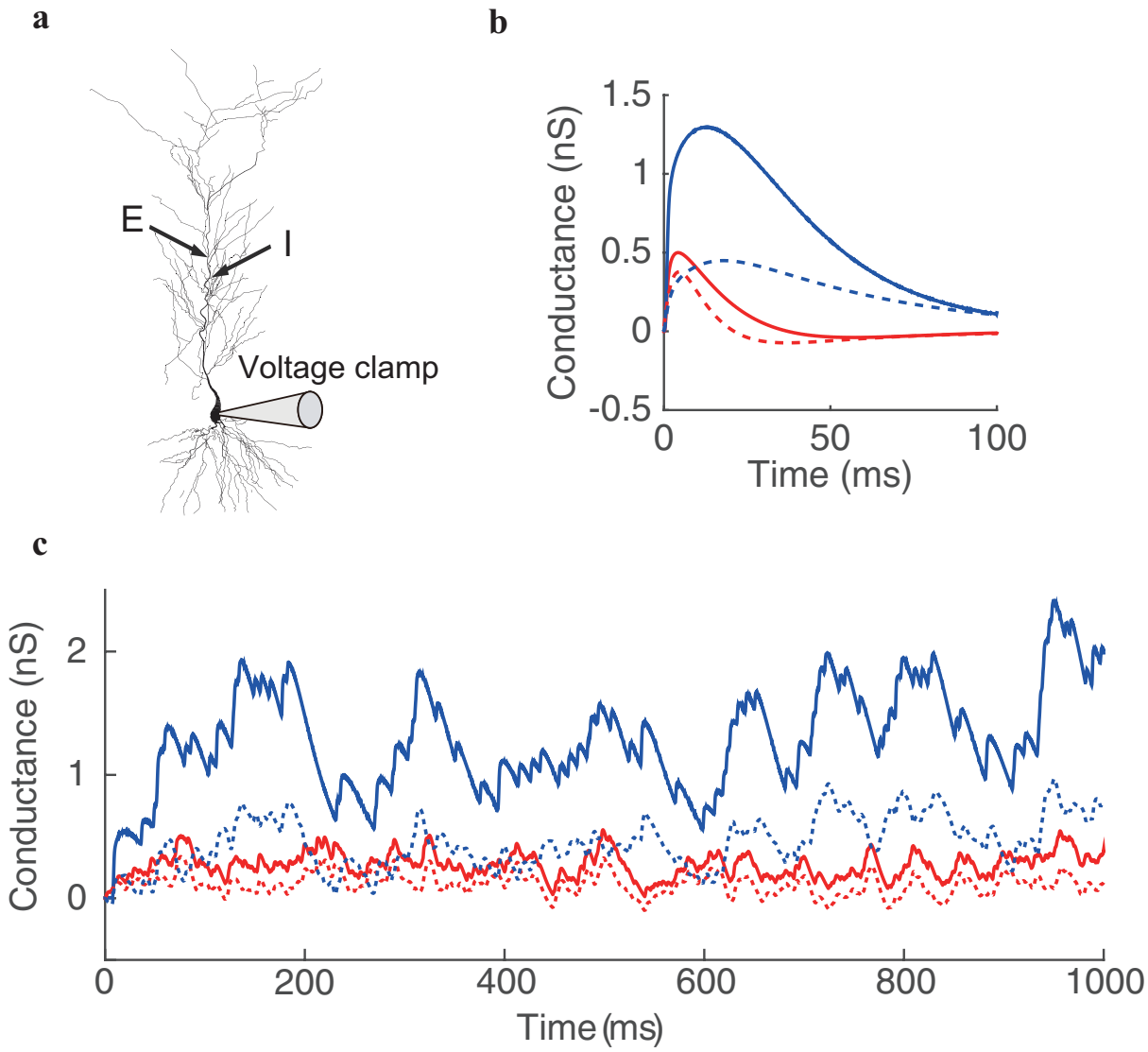

Fig. S4. The issue of conductance measurement based on the assumption of linear summation of E and I synaptic currents. **a**, the recording configuration when the realistic neuron model receives a pair of E and I inputs. A voltage clamp is made at the soma. Somatic voltage is clamped from -60 mV to -100 mV with a decrement of -10 mV when both the E and I inputs are given simultaneously at the dendritic trunk 350 μm and 280 μm away from the soma. The arrows indicate the locations of the E and I inputs. **b**, the recovered E conductance (dash red) and I conductance (dash blue) based on the form of linear summation of E and I synaptic currents when a pair of transient E and I inputs are given simultaneously at the locations indicated in **a**. The reference E conductance (solid red) and I conductance (solid blue) are calculated from the point neuron model when the E or I input is given separately in the realistic neuron model. **c**, the same as **b** except that the neuron receives two spike trains as the inputs. The input times at each location are uniformly distributed from 0 ms to 1000 ms. The rate of the E input is 400 Hz and that of the I input is 100 Hz at each input location.

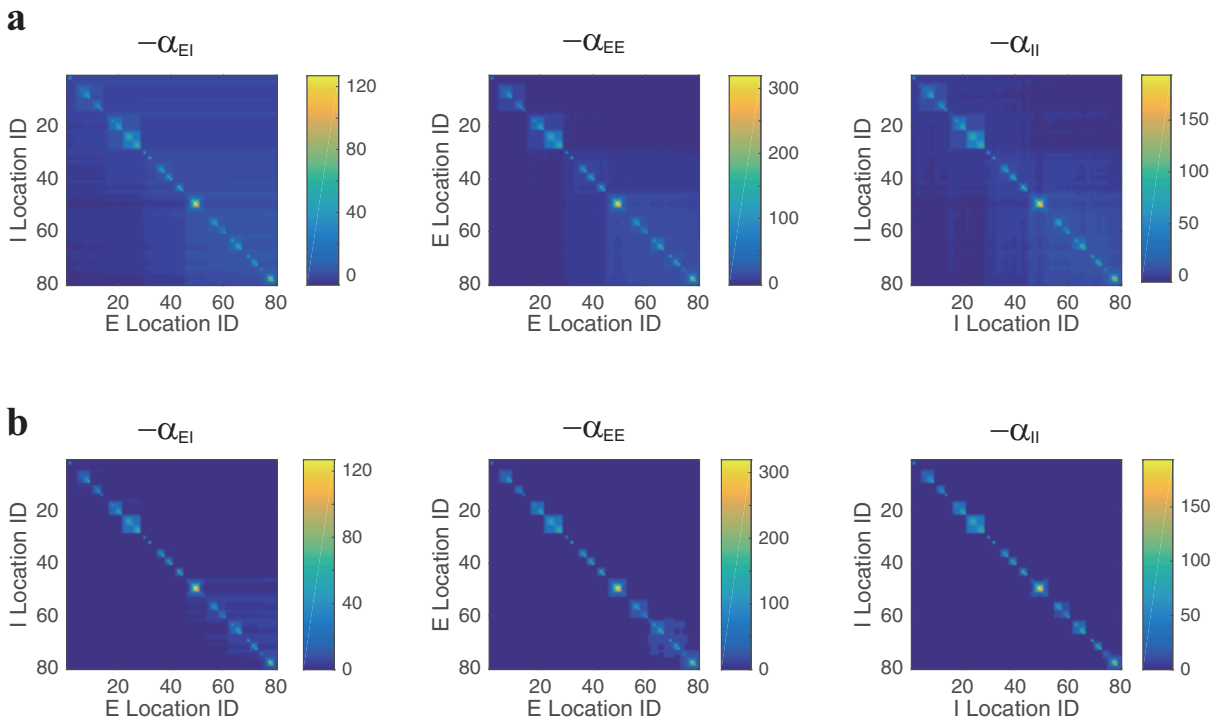

Fig. S5. The sparsity of the integration coefficient matrices. **a**, the measured integration coefficient matrices for $-\alpha_{EI}$, $-\alpha_{EE}$, and $-\alpha_{II}$. An element in each matrix corresponds to an integration coefficient measured in the realistic neuron model given a pair of inputs at its dendritic arbor in *stratum radiatum*. The labels of the x-axis and the y-axis of each matrix are the ID number of the dendritic compartment in the model. In general, two compartments are physically close to each other if their ID numbers are close, and one compartment is further away from the soma than another compartment if its ID number is larger than that of another compartment. **b**, the same as **a** except that the minus of the coefficients below a threshold in each matrix are set to be zero. The thresholds are determined as that the integration coefficient is significantly nonzero such that the bilinear integration of synaptic currents only leads to a change of SSP greater than 5%, given an EPSP of 4 mV and an IPSP of -1 mV. The value of the threshold is 3.13 k$\Omega \cdot \mathrm{cm}^2$ for the E-I case, 16.72 k$\Omega \cdot \mathrm{cm}^2$ for the E-E case, and 9.89 k$\Omega \cdot \mathrm{cm}^2$ for the I-I case. The percentage of nonzero coefficients in each matrix is 15.33% for the E-I case, 7.39% for the E-E case, and 4.67% for the I-I case, which is sparse.

References

1. Koch C (2004) *Biophysics of computation: information processing in single neurons.* (Oxford university press).
2. Hao J, Wang Xd, Dan Y, Poo Mm, Zhang Xh (2009) An arithmetic rule for spatial summation of excitatory and inhibitory inputs in pyramidal neurons. *Proceedings of the National Academy of Sciences* 106(51):21906–21911.
3. Zhou D, Li S, Zhang Xh, Cai D (2013) Phenomenological incorporation of nonlinear dendritic integration using integrate-and-fire neuronal frameworks. *PloS one* 8(1):e53508.
4. Li S, Liu N, Zhang Xh, Zhou D, Cai D (2014) Bilinearity in spatiotemporal integration of synaptic inputs. *PLoS computational biology* 10(12):e1004014.
5. Barlow HB, Hill RM (1963) Selective sensitivity to direction of movement in ganglion cells of the rabbit retina. *Science* 139(3553):412–412.
6. Vaney DI, Taylor WR (2002) Direction selectivity in the retina. *Current opinion in neurobiology* 12(4):405–410.
7. Agmon-Snir H, Carr CE, Rinzel J (1998) The role of dendrites in auditory coincidence detection. *Nature* 393(6682):268.